Soft Matter

Accepted Manuscript

This article can be cited before page numbers have been issued, to do this please use: I. Gleria, E. Mocskos and M. Tagliazucchi, *Soft Matter*, 2017, DOI: 10.1039/C6SM02725C.

ROYAL SOCIETY OF CHEMISTRY

rsc.li/soft-matter-journal

View Article Online
DOI: 10.1039/C6SM02725C

Soft Matter

ARTICLE

Minimum Free-Energy Paths for the Self-Organization of Polymer Brushes

Received 00th January 20xx,
Accepted 00th January 20xx

DOI: 10.1039/x0xx00000x

www.rsc.org/

Ignacio Gleria,[a] Esteban Mocskos[a,b] and Mario Tagliazucchi*,[c,d]

A methodology to calculate minimum free-energy paths based on the combination of a molecular theory and the improved string method is introduced and applied to study the self-organization of polymer brushes in poor solvent conditions. Polymer brushes in a poor solvent cannot undergo macroscopic phase separation due to the physical constraint imposed by the grafting points; therefore, they microphase separate forming aggregates. Under some conditions, the theory predicts that the homogeneous brush and the aggregates can exist as two different minima of the free energy. The theoretical methodology introduced in this work allows to predict the minimum free-energy path connecting these two minima as well as the morphology of the system along the path. It is shown that the transition between the homogeneous brush and the aggregates may involve a free-energy barrier or be barrierless depending on the relative stability of the two morphologies and the chain length and grafting density of the polymer. In the case where a free-energy barrier exists, one of the morphologies is a metastable structure and, therefore, the properties of the brush as the quality of the solvent is cycled are expected to display hysteresis. The theory is also applied to study the adhesion/deadhesion transition between two opposing surfaces modified by identical polymer brushes and it is shown that this process may also requiere to surpass a free-energy barrier.

Introduction

Soft materials exhibit a subtle competition between physical interactions, chemical equilibria and entropic forces that enables their self-assembly into organized structures.[1-4] Block-copolymers,[5-7] amphiphilic molecules[3, 8] and colloids[9, 10] are typical examples of soft materials that exhibit rich self-assembly behaviours. Due to the complexity of their free-energy landscapes, self-assembled soft materials are, in many cases, in metastable states (*i.e.* local minima of the free energy) rather than in thermodynamic equilibrium (global minimum of the free energy). The relaxation from a metastable state towards equilibrium must proceed through a free-energy barrier and, therefore, it can be very slow if the height of the barrier is large enough compared with the available thermal energy (k_BT). Understanding the parameters that control the free-energy barriers between different structures in soft material is of prime importance because these barriers can be used to stabilize a desired metastable structure, but also because they may trap the system into an undesired metastable state thus preventing to obtain the desired equilibrium morphology.

Thin layers of end-grafted polymers, known as polymer brushes,[11] in a poor solvent self-organize into aggregates of different shape, such as micelles, stripes and continuous layers with solvent-filled holes.[1, 12-25] Self-assembly in polymer brushes results from the fact that physical grafting of the polymers to the substrate prevents macroscopic phase separation in a poor solvent, therefore the polymers aggregate into microscopic structures, in a process known as microphase separation.[1, 12, 14] Microphase separation of single-component or mixed polymer brushes is appealing for applications in smart surfaces[23] and nanoparticles,[26-28] bottom-up patterning[24] and nanoparticle motion.[29]

In the past, the self-organization of polymer brushes in a poor solvent has been theoretically studied with self-consistent-field theories (SCF),[12, 13, 19] scaling arguments,[12, 14, 30] molecular theories[1, 15, 31] and computer simulations.[16-18] These studies not only identified the different equilibrium morphologies, but also evidenced the presence of metastable states: in some cases more than one possible morphology can be obtained under the same conditions.[15, 30] In those cases, the morphology with the lowest free energy corresponds to the equilibrium structure, whereas the other morphologies are metastable states. So far, the free-energy barriers between these states remain completely unexplored.

[a] Universidad de Buenos Aires. Facultad de Ciencias Exactas y Naturales, Departamento de Computación. Buenos Aires, Argentina.
[b] CONICET. Centro de Simulación Computacional para Aplicaciones Tecnológicas (CSC). Buenos Aires, Argentina.
[c] Universidad de Buenos Aires. Facultad de Ciencias Exactas y Naturales, Departamento de Química Inorgánica, Analítica y Química-Física. Buenos Aires, Argentina. E-mail: mario@qi.fcen.uba.ar
[d] CONICET-Universidad de Buenos Aires. Instituto de Química Física de los Materiales, Medio Ambiente y Energía (INQUIMAE). Buenos Aires, Argentina.

Electronic Supplementary Information (ESI) available: Discretization and Numerical Solving of the Theory and Numerical Confirmation that the Barriers in the MFEP are Saddle Points of the Free-Energy Functional. See DOI: 10.1039/x0xx00000x

View Article Online
DOI: 10.1039/C6SM02725C

In this work, we derived a molecular theory for the calculation of minimum free-energy paths (MFEP) and used it to explore the free-energy landscape of self-organized polymer brushes. Our theory is a combination of a molecular theory for soft materials at interfaces[1, 32, 33] and the improved string method for minimal energy paths.[34] The improved string method has been used before in combination with simulations and SCF theories to explore lipid bilayers,[35-37] block copolymers[38-41] and the collapse of a single hydrophobic chain in solution.[27] The present work reports its first application to study the self-organization of polymer brushes. We examined the transition between a homogeneous brush and self-organized polymer aggregates and found that this transition may have a free-energy barrier, whose height increases for increasing chain length and surface coverage, or be barrierless. Our results support the idea that metastable states may be relevant in experiments and that the processing history of a self-assembled polymer brush may play an important role in dictating its morphology. We also considered systems comprising two opposing surfaces modified by identical polymer-brush layers. In this case, we observed a free-energy barrier for the adhesion/deadhesion process, which may be related to the hysteresis observed for this process in AFM-colloidal-probe and surface-force-apparatus experiments.

Methods

Molecular Theory

We start by deriving the molecular theory for (meta)stable states, which is formulation of the theory developed by Szleifer and collaborators for the case neutral polymer brushes on flat surfaces.[1, 32, 33] We consider N_p linear polymer chains of L monomers per chain that are end-grafted to a surface of total area A. We propose the following free-energy functional for this system:

$$\beta W = \int \rho_s(\mathbf{r})\left(\ln(\rho_s(\mathbf{r})v_s)-1\right)d\mathbf{r} + \sum_{j=1}^{N_p}\sum_{\alpha=1}^{Nconf} P(j,\alpha)\ln\left(P(j,\alpha)\right) - \iint \frac{\beta\varepsilon}{2} g(|\mathbf{r}-\mathbf{r}'|)\left\langle\rho_p(\mathbf{r})\right\rangle\left\langle\rho_p(\mathbf{r}')\right\rangle d\mathbf{r}d\mathbf{r}' \quad (1)$$

where $\beta = 1/k_BT$ and k_B is Boltzmann's constant. The first term in eq (1) is the free energy due to the translational entropy of the solvent molecules, in this term $\rho_s(\mathbf{r})$ is the number density of solvent molecules at position $\mathbf{r}$ and v_s is the molecular volume of a solvent molecule (we used v_s = 0.03 nm^3). The second term is the free-energy contribution due to the conformational entropy of the polymer chains, where $P(j, \alpha)$ is the probability of having chain j (j=1,N_p) in conformation α. The sum over α runs, in principle, over all possible polymer conformations, although in practice we use a very large representative set of size N_{conf} that we generate using the rotational isomeric model.[32] The last term in eq (1) accounts for the Van der Waals (VdW) effective attractive energy between polymer beads.[1, 32] In this term, ε is the strength of the attractive interactions, *i.e.* a measure of the hydrophobicity (larger ε corresponds to stronger effective VdW attractions), $g(|\mathbf{r}-\mathbf{r'}|)$ is a function that describes the distance dependence of the VdW attractions and $\langle\rho_p(\mathbf{r})\rangle$ is the average number density of the polymer segments at $\mathbf{r}$, given by:

$$\left\langle\rho_p(\mathbf{r})\right\rangle = \sum_{j=1}^{N_p}\sum_{\alpha=1}^{Nconf} P(j,\alpha)n_p(\alpha,\mathbf{r},j) \quad (2)$$

where $n_p(\alpha,\mathbf{r},j)d\mathbf{r}$ is the number of segments that chain j has in the volume element between $\mathbf{r}$ and $\mathbf{r}+d\mathbf{r}$ when it is in conformation α. Note that eq (1) does not contain a term for the repulsive interactions. Repulsions are modelled as excluded-volume interactions and are accounted for exactly for monomers within the same chain during the generation of the set of polymer conformations and, for all other cases, approximately using a packing constraint,

$$\left\langle\rho_p(\mathbf{r})\right\rangle v_p + \rho_s(\mathbf{r})v_s = 1 \quad (3)$$

where v_p is the volume of a polymer segment (we used v_p = 0.11 nm^3). Finally, the probabilities for each j must be normalized, namely,

$$\sum_{\alpha=1}^{Nconf} P(j,\alpha) = 1 \quad (4)$$

In principle, the free energy in eq (1) is a functional of the number density of the solvent, $\rho_s(\mathbf{r})$, and the probability distribution function of chain conformations, $P(j,\alpha)$. Note, however, that the packing constraint reduces the number of degrees of freedom of the system: given $P(j,\alpha)$, the number density of the polymer segments can be determined through eq (2), which unequivocally fixes the number density of the solvent $\rho_s(\mathbf{r})$ via the packing constraint, eq (3). In previous works,[1, 32, 33] the packing constraint was enforced with the aid of a Lagrange multiplier $\beta\pi(\mathbf{r})$. If one chooses this approach, then $\rho_s(\mathbf{r})$ and $P(j,\alpha)$ remain as thermodynamically independent variables. However, for the molecular theory/string method described below it is convenient to reduce the number of thermodynamically independent variables and, therefore, we choose here to replace eqs (2) and (3) into the free energy, eq (1), in order to eliminate $\rho_s(\mathbf{r})$ (the final result of this approach is identical to that obtained using Lagrange multipliers). In the case of the probability normalization constraint, eq (4), one can again choose to replace it into eq (1), thus reducing the number of thermodynamically independent $P(j,\alpha)$ variables by one for each j. However, since this approach only slightly reduces the number of thermodynamically independent variables but adds complexity to the problem, we found it more convenient to use in this case a Lagrange multiplier in order to enforce eq (4), namely we will minimize the following free-energy functional:

$$\beta F = \beta W + \sum_{j=1}^{N_p}\left[\xi(j)\left(\sum_{\alpha=1}^{Nconf} P(j,\alpha)-1\right)\right] \quad (5)$$

where $\xi(j)$ is the Lagrange multiplier enforcing probability normalization for chain j. The extremum of F with respect to $P(j,\alpha)$ yields,

View Article Online
DOI: 10.1039/C6SM02725C

$$\frac{\partial \beta F}{\partial P(j,\alpha)} = \ln P(j,\alpha) + \ln(q(j)) + \int n_p(\alpha,\mathbf{r},j)\left(-\frac{v_p}{v_s}\left(\ln(\rho_s(\mathbf{r})v_s)\right) - \int \beta\varepsilon g(|\mathbf{r}-\mathbf{r}'|)\langle\rho_p(\mathbf{r}')\rangle d\mathbf{r}'\right)d\mathbf{r} = 0 \quad (6)$$

where $q(j) = \exp(\xi(j)+1)$ is the single-chain partition function of chain *j*. We now define:

$$\beta\pi(\mathbf{r}) = -\frac{1}{v_s}\ln(\rho_s(\mathbf{r})v_s) \quad (7)$$

as the local osmotic pressure based on results in previous work[1, 32, 33] and then replace this definition in eq. (6). Following this step and further rearranging of eq (6), we obtain,

$$P(j,\alpha) = \frac{1}{q(j)}\exp\left[-\int n_p(\alpha,\mathbf{r},j)\left(v_p\beta\pi(\mathbf{r}) - \int \beta\varepsilon g(|\mathbf{r}-\mathbf{r}'|)\langle\rho_p(\mathbf{r}')\rangle d\mathbf{r}'\right)d\mathbf{r}\right] \quad (8)$$

In order to solve the theory, the set of equations (2), (3), (7) and (8) are discretized in a lattice and numerically solved.[33]

Derivation of the Molecular Theory/String Method

The procedure described in the previous section allows to calculate the structure and thermodynamics of an equilibrium or metastable system. In order to study the transition between these (meta)stable states, we will combined the molecular theory with the improved string method developed by Weinan *et al*.[34] to calculate minimum free-energy paths (MFEPs). The MFEP connects two points on the free-energy hypersurface, *i.e.* the hypersurface given by the free energy as a function of the coordinates that describe the state of the system. As we discussed above, the free-energy functional *F* in the present formulation of the molecular theory is a function of $P(j,\alpha)$ only. Let us consider a more general theoretical framework where the coordinates are given by a transformation of $P(j,\alpha)$, *e.g.* considering $\Omega(j,\alpha)$ coordinates with $\Omega(j,\alpha) = f(P(j,\alpha))$, where $f(x)$ is an invertible function in the interval $0 < x < 1$. Generally speaking, the MFEP on the $F(P(j,\alpha))$ hypersurface is different to that on the $F(\Omega(j,\alpha))$ hypersurface, however the local extrema of both MFEPs (which correspond to extrema or saddle points of *F*) are exactly the same due to the relationship,

$$\frac{\partial \beta F}{\partial P(j,\alpha)} = \frac{\partial \beta F}{\partial \Omega(j,\alpha)}\frac{\partial f(P(j,\alpha))}{\partial P(j,\alpha)} \quad (9)$$

which implies that $\partial\beta F/\partial\Omega(j,\alpha) = 0$ only if $\partial\beta F/\partial P(j,\alpha) = 0$. The use of $\Omega(j,\alpha)$ instead of $P(j,\alpha)$ is advantageous because an adequate choice of *f* can greatly accelerate the convergence of the numerical problem. We empirically found that using $f(x) = x^{1/2}$ provides stable and fast converge, thus we used that parametrization in the calculations. We stress that the choice of *f* does not affect the existence, free energy and morphology of the barriers and local minima in the MFEP. As a consistency check, we verified that the extrema of the MFEP calculated using our choice of *f* are in fact saddle points of *F* by numerically checking that they fulfil eq (6), see Electronic Supplementary Information.

By definition,[42] the MFEP is a curve on a hypersurface for which the normal components of ∇F are zero, where ∇ is the gradient operator. In order to properly sample the MFEP, we start with a trial string (a path on the free energy hypersurface that is not the MFEP) that we generate by linear interpolation of $\Omega(j,\alpha)$ between the initial and final states. These two states are obtained using the molecular theory for (meta)stable states described in the previous section and we fix them during the MFEP calculation. We divide the string in *M*-1 segments determined by *M* nodes. We have used *M* between 20 and 40 in the calculations, which is enough to guarantee that our results are converged with respect to *M*. The string becomes unequivocally determined by the set of values of $\Omega(j,\alpha)$ at the nodes, which we denote $\Omega^k(j,\alpha)$ with $k = 1$ to *M*. We will require that in the MFEP the arc length between two neighbouring nodes is equal to a constant value, L_0 (constant arc-length parametrization[34]), *i.e.*

$$\sum_{j=1}^{N_p}\sum_{\alpha=1}^{Nconf}\left|\Omega^k(j,\alpha) - \Omega^{k-1}(j,\alpha)\right| = S(k) - S(k-1) = L_0 \quad (10)$$

where we define $S(k)$ as the position of node *k* along the MFEP. We set $S(1) = 0$ and then $S(k)$ is required to be

$$S(k) = \sum_{l=2}^{k}\left(\sum_{j=1}^{N_p}\sum_{\alpha=1}^{Nconf}\left|\Omega^l(j,\alpha) - \Omega^{l-1}(j,\alpha)\right|\right) = (k-1)L_0 \quad (11)$$

The total arc-length of the string is required to be $S(M) = (M-1)L_0$ (position of last node).

Weinan *et al.*[34] showed that the MFEP fulfills the condition:

$$-\frac{\partial \beta F}{\partial \Omega^k(j,\alpha)} + \lambda(k)\left(\sum_{j=1}^{N_p}\sum_{\alpha=1}^{Nconf}\left|\Omega^k(j,\alpha) - \Omega^{k-1}(j,\alpha)\right| - L_0\right) = 0 \quad (12)$$

for each *j* and α. In this equation, $\lambda(k)$ is a Lagrange Multiplier enforcing eq (10) for each *k*, which can be regarded as the tension of the string at position *k*. In the improved string method,[34] the Lagrange multipliers $\lambda(k)$ are not determined, but rather condition (10) is enforced by interpolation steps. In other words, given an initial string connecting two fixed ends on the free-energy hypersurface, we first evolve the system a small time step according to the equation

$$\frac{d\Omega^k(j,\alpha)}{dt} = -\frac{\partial \beta F}{\partial \Omega^k(j,\alpha)} \quad (13)$$

where the right hand side is calculated by isolating $\partial\beta F/\partial\Omega(j,\alpha)$ from eq (9) and replacing $\partial\beta F/\partial P(j,\alpha)$ using the expression derived in eq (6). After this step, we enforce the normalization of the probabilities of chain *j*, and, then, we determine the position of the nodes as:

View Article Online
DOI: 10.1039/C6SM02725C

$$S'(k) = \sum_{l=2}^{k} \left(\sum_{j=1}^{N_p} \sum_{\alpha=1}^{Nconf} \left| \Omega^{l}(j,\alpha) - \Omega^{l-1}(j,\alpha) \right| \right) \quad (14)$$

(where $S'(1) = 0$). In general, the position of the nodes after the evolution step will not fulfil eq (11), therefore, we use the $\Omega^k(j,\alpha)$ vs $S'(k)$ data to interpolate new values of $\Omega^k(j,\alpha)$ at the positions $S(k)$ given by eq (11) (using $L_0 = S'(M)/(M\text{-}1)$). The evolution/interpolation steps are then repeated until convergence. When the stationary point is reached, the displacement of $\Omega^k(j,\alpha)$ during the evolution step cancels that introduced by the interpolation step. The interpolation step (in the limit of a large number of nodes) is tangential to the string, therefore, the displacement of $\Omega(j,\alpha)$ normal to the string during the evolution step should vanish.[34, 43] According eq. (13), this condition requires the gradient of F in the direction normal to the string to be zero, which, by definition, corresponds to a MFEP.

It is important to mention that the calculation of the MFEP is computationally much more demanding than the calculation of the (meta)stable states; therefore we have optimized our numerical implementation in order to deal with the increase in computational requirements. In a typical calculation, we use $N_P \sim 20$ different chains (grafting points) in the system and a set of $N_{conf} = 2.5{\cdot}10^5$ conformations, thus $\Omega(j,\alpha)$ has $\sim 5{\cdot}10^6$ elements. The evaluation of the vector $\partial\beta F/\partial\Omega(j,\alpha)$ is the bottleneck of the MFEP calculation. In the Electronic Supplementary Information, we show that this calculation requires the multiplication of sparse matrices and discuss the use of a high-performance numerical library for this calculation. It is also important to mention that we introduced the theory for the most general case of a system having inhomogeneities in the three spatial dimensions, however, in order to perform the calculations, we assumed inhomogeneities in only two dimensions (one parallel and one perpendicular to the substrate). This assumption greatly decreases the number of local free energy minima and lowers the computational cost of the calculations. In the calculations, we used periodic boundary conditions in the direction parallel to the substrate.

Results

Transition from Homogeneous Brush to Self-Assembled Aggregates

Let us consider the system schematized in Figure 1A, where polymer chains are end-tethered to a flat surface. Solving the molecular theory for this system (under the assumption of heterogeneities in the x and y directions only, see Figure 1A) yields two types of structures: homogeneous brushes (panel *h* in Figure 1B) and self-assembled aggregates of chains (panel *a* in Figure 1B). The relative thermodynamic stability of these two morphologies has been addressed in previous works,[1, 12, 14, 15] however the free-energy barriers between them remain uncharacterized

The free-energy per chain in the case of a self-assembled aggregate depends on the size of the aggregate; therefore, before examining the MFEP between the homogeneous and the self-organized brushes, we need to determine the optimal size of the assemblies. In the present formulation of the molecular theory the size of the aggregates can be controlled by the size of the calculation box in the dimension parallel to the substrate (x axis), for example in Figure 1B we have fixed the lateral size of the system to 10 nm. The full black curve in Figure 2A shows the free energy per chain ($\beta F/N_P$) as a function of the size of the aggregate (D) for a typical set of calculation parameters. The minimum of the curve indicates the optimal aggregate size, D^{opt}. The optimal aggregate size results from the balance between the surface energy of the polymer/solvent interface, which is optimized for small area/volume ratios and, therefore, large spherical assemblies, and the entropic penalty associated to stretching chains that are grafted far from the centre of the aggregate, which is optimized for small assemblies.[12, 14, 15, 26] The dashed blue line in Figure 2A shows the free energy of the homogeneous brush, which, as expected, is independent of the size of the calculation box. In the example of Figure 2, the self-assembled aggregate has an optimal size D^{opt} = 10 nm and a free energy per chain that is 0.11 k_BT smaller than that of the homogeneous brush.

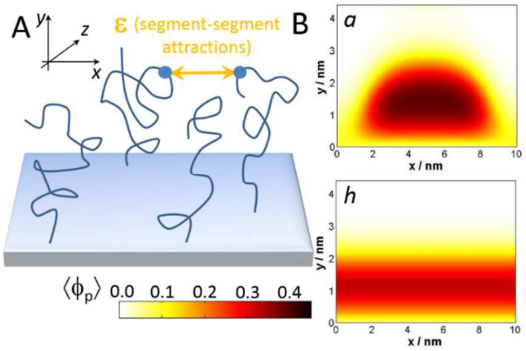

Figure 1: A. Scheme showing the system under study: polymers of length L are end-grafted to a planar surface with surface density N_P/A. The monomers of the polymers have attractive effective Van der Waals interactions, whose strength is given by the parameter ε. B. Color maps showing the volume fraction of the polymer in the x-y plane for the system in A for two different morphologies: aggregates (*a*) and homogeneous brush (*h*). These two morphologies correspond to two local minima of the free energy for the same calculation conditions (N_P/A = 0.1 chains·nm^{-2}, L = 50 monomers/chain, ε = 0.875 k_BT).

Figures 2B and 2C show that the optimal size increases both for increasing chain length of the polymer, L, and the grafting density, N_P/A, in qualitative agreement with scaling arguments in the literature.[12] These trends are explained by the fact that increasing L or N_P/A increases the number of monomers in the aggregate without increasing the stretching penalty and, thus, lead to an increase of the optimal aggregate size. On the other hand, the strength of segment-segment VdW attractions, ε, has almost no effect on the optimal size (Figure 2D). Increasing ε increases the density in the centre of the aggregate, thus incrementing the stretching penalty of chains grafted far from the centre (which would favour smaller assemblies). However, increasing ε also results in a higher solvent/polymer interfacial energy, which would favour large assemblies in order to decrease the area/volume ratio of the aggregate. Both effects cancel, so that the optimal size of the self-assembled aggregate is approximately unaffected by ε in the range of conditions studied.

View Article Online
DOI: 10.1039/C6SM02725C

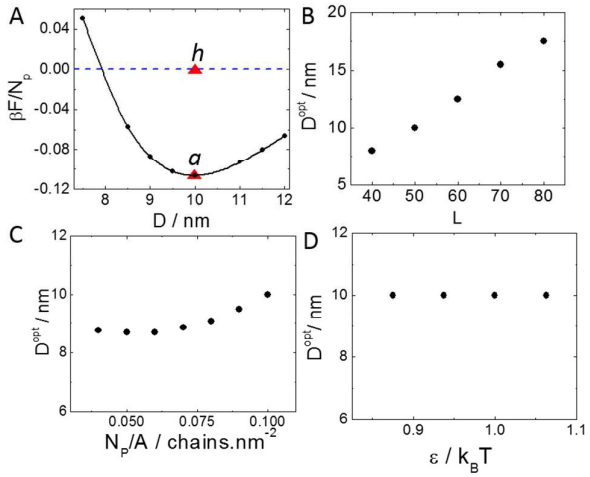

Figure 2: A. Free energy per chain for the aggregates (black solid line) and the homogeneous brush morphology (blue dashed line) as a function of the size of the calculation box in the x dimension. The red triangles indicate the position of the morphologies shown in Figure 1B (*a* = aggregate, *h* = homogeneous brush). B-D. Optimal aggregate size as a function of chain length (B), surface coverage (C) and effective strength of Van der Waals attractions (D). Calculation conditions: L = 50 (except panel B), N_P/A = 0.1 chains·nm^{-2} (except panel C) and ε = 0.875 k_BT (except panel D).

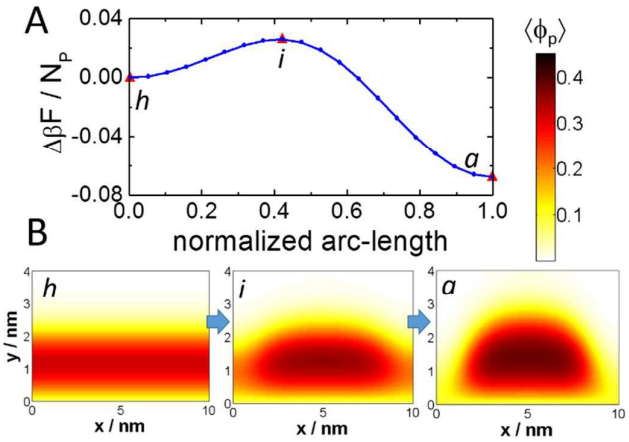

Figure 3: A. Minimum free-energy path (free energy as a function of string arc-length) for the transition from the homogeneous brush (*h*) to the self-assembled aggregates (*a*). These two morphologies correspond to two different local minima of the free energy for the same calculation conditions (L = 50, N_P/A = 0.1 chains·nm^{-2} , ε = 0.87 k_BT) B. Color maps showing the volume fraction of the polymer for the morphologies indicated with red triangles in panel A.

Using the optimal aggregate size determined above, we focused on the minimum free-energy path (MFEP) for the transition from the homogeneous brush to the self-assembled aggregates ($h \rightarrow a$). Figure 3A shows a typical MFEP for this transition (we have chosen the *h* state as the reference state, thus it has zero free energy in all conditions). In the example Figure 3A, the aggregates are more stable than the homogeneous brush by 0.068 k_BT/chain, which corresponds to a difference of 0.68 k_BT per aggregate, assuming that the assemblies will have the same size in the *x* and *z* directions (in this case, the aggregate size is 10 nm, see panel *a* in Figure 3B). The transition between the morphologies requires to surpass a barrier of 0.026 k_BT/chain (0.26 k_BT/aggregate). Figure 3B shows the morphology of the system in the *a* and *h* states, as well as in the barrier state (panel *i*).

Figure 4 shows the effect of the relative stability of the *h* and *a* morphologies on the height of the free-energy barrier. The black curve with diamond symbols in Figure 4A corresponds to the condition where *a* and *h* have the same free energy. Increasing the VdW attraction energy (ε) stabilizes the aggregates with respect to the homogeneous brush. As the free-energy of the self-assembled aggregates decreases, the barrier for the $h \rightarrow a$ transition decreases until it completely vanishes (see red curve with circle symbols in Figure 4A). Once the $h \rightarrow a$ becomes barrierless for sufficiently large ε (sufficiently strong VdW attractions), the homogenous brush can no longer exists as a metastable state of the system and microphase separation cannot be avoided. Therefore, microphase separation of the homogeneous brush into self-assembled aggregates may exhibit a barrier (activated process) or be barrierless. In analogy to macroscopic phase separation,[44] one can expect that the activated process will require the formation of critical nuclei of a few aggregates from the homogeneous brush, similar to a binodal decomposition, while the barrierless process would result in a homogeneous microphase separation similar to a spinodal decomposition.

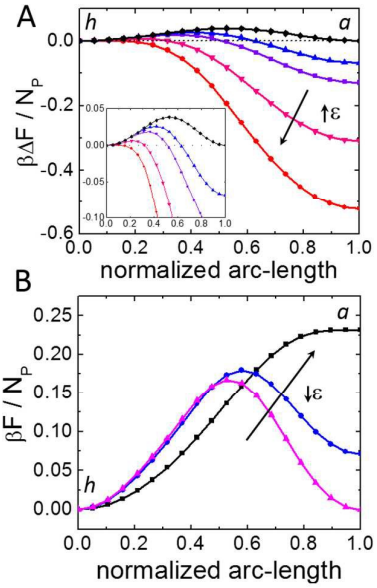

Figure 4: A. Minimum free-energy paths for the transition from the homogeneous brush (*h*) to the self-assembled aggregates (*a*) for L = 50, N_P/A = 0.1 chains·nm^{-2} and different values of ε (in the direction of the arrow, ε/k_BT = 0.864, 0.870, 0.875, 0.888 and 0.900). The inset shows an enlarged plot of the barrier region. B. Same as A for L = 50, N_P/A = 0.125 chains·nm^{-2} and ε/k_BT (in the direction of the arrow) = 0.932, 0.925 and 0.906. In all cases, we set the free-energy reference to be zero for the homogeneous brush morphology.

In Figure 4B, we analyse the case where the aggregates are thermodynamically less stable than the homogenous brush. As the stability of the homogeneous brush is increased by decreasing ε, we observe that the barrier for the aggregate to homogeneous brush ($a \rightarrow h$) transition decreases, until the process becomes barrierless. In other words, both the $h \rightarrow a$

View Article Online
DOI: 10.1039/C6SM02725C

and the $a \rightarrow h$ transitions can be activated or barrierless processes. Therefore, the theory predicts that there is a range of ε where both the self-organized aggregates and the homogenous brush coexist (one of them as the stable morphology and the other as a metastable morphology) and that for values of ε below or above this coexistence region, only the *h* and *a* morphologies, respectively, can exist.

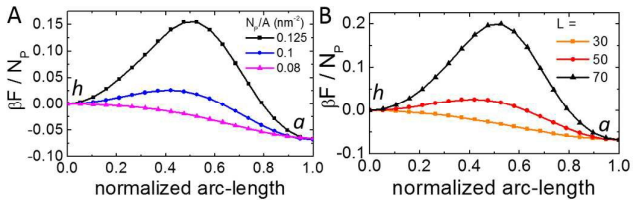

Figure 5: A. Minimum free-energy paths for the transition from a homogeneous brush (*h*) to self-assembled aggregates (*a*) for L = 50 and different values of N_P/A. The value of ε for each curve was chosen in order to ensure a constant free-energy difference between the aggregates and homogeneous brush, ε/k_BT = 0.833 (N_P/A = 0.08 chains·nm^{-2}), 0.870 (N_P/A = chains·0.1 nm^{-2}) and 0.938 (N_P/A = chains·0.125 nm^{-2}). B. Same as A for N_P/A = 0.125 chains·nm^{-2}, different values of L and ε/k_BT = 0.896 (L = 30), 0.870 (L = 50) and 0.892 (L = 70).

It is important to address how the transition barrier depends on the properties of the system, such as the chain length of the polymer (L) and its surface density (N_P/A). Since we have shown in Figure 4 that this barrier strongly depends on the difference of free energy between the *a* and *h* morphologies, we decided to compare systems where L and N_P/A vary but the *a*-*h* free-energy difference (which we controlled by changing ε, the effective VdW attraction strength) is constant. We observe that increasing either N_P/A (Figure 5A) or L (Figure 5B) increases the height of the transition barrier. The results in Figure 5B show that the free energy at the barrier can be as large as 0.2 k_BT/chain (4.8 k_BT/aggregate) for L = 70. Since this chain length is in the lower range of those used in experiments,[21, 26] we expect that the formation of metastable states in self-organized polymer brushes will be relevant in experimental realizations.

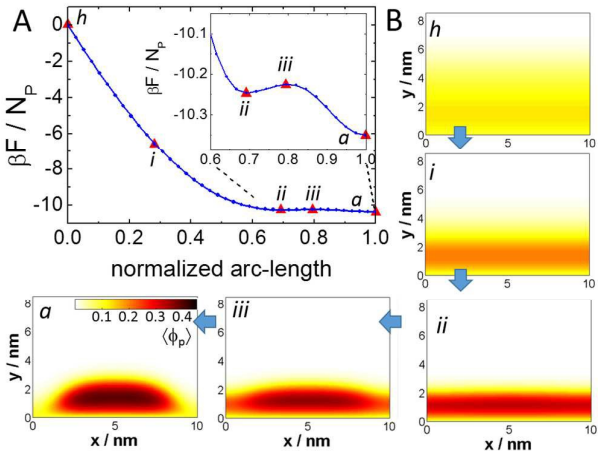

Figure 6: A. Minimum free-energy path for ε = 0.875 k_BT from a homogeneous brush (*h*) equilibrated at ε = 0.5 k_BT to self-assembled aggregates (*a*) equilibrated at ε = 0.875 k_BT. B. Color maps showing the volume fraction of the polymer for the morphologies indicated with red triangles in panel A. Calculation parameters L = 50, N_P/A = 0.1 chains·nm^{-2}.

Minimum Free-Energy Paths Starting from Unstable States

The MFEPs in Figures 3, 4 and 5 connect stable morphologies that are different local minima of the free energy for the same calculation conditions. In experiments, however, the polymer brush would be initially in a good solvent and then microphase separation will be triggered by rapidly reducing the quality of the solvent by replacing the solvent or adding a co-solvent to the solution in contact with the brush.[26] Since the brushes under study are very thin (~ 2-6 nm), replacement of solvent molecules within the brush is expected to be fast compared to the reorganization of the polymer chains. Therefore, the self-organization transition will involve a transition starting from an unstable morphology that it is not a local minimum of the free energy. Figure 6A shows a calculation where the starting morphology is fixed to a homogeneous brush equilibrated in a relatively good solvent (ε = 0.5 k_BT), but the MFEP and the final aggregated state correspond to poor solvent conditions (ε = 0.875 k_BT). Note the non-zero slope of the MFEP in the initial *h* state that indicates that this state is not a minima of the free energy. Interestingly, the MFEP shows that the $h \rightarrow a$ transition occurs in two well-defined steps. First, the brush morphology equilibrated in a good solvent barrierlessly collapses to the homogeneous brush equilibrated at the current solvent quality (morphology *ii*), which is a local minima of the free energy under the conditions of Figure 6. In the second step, the collapsed homogeneous brush (morphology *ii*) microphase separates forming aggregates (morphology *a*) via an activated process. Interestingly, Figure 7A shows that the two-step transition persists even if the quality of the solvent is lowered to ε = 0.925 k_BT, where the collapsed homogenous brush is no longer a local minima of the free energy (see Figure 4A). In other words, the MFEP in Figure 7A, where a brush equilibrated at ε = 0.5 k_BT is collapsed at ε = 0.925 k_BT, shows a monotonic decrease of the free energy along the transition; however the morphologies of the system (see sequence of blue arrows in Figure 7C) show that the transition effectively occurs via a two-step process: first collapsing the homogeneous brush (panels *h*, *i* and *ii* in Figure 7C) and then forming the aggregates (panels *iii* and *a* in Figure 7C). In Figure 7B, we show the MFEP for a process that is the inverse of that in Figure 7A: aggregates equilibrated in poor solvent (ε = 0.925 k_BT) are allowed to swell in a good solvent (ε = 0.5 k_BT) in order to yield the homogeneous brush in good solvent. In this case, the morphologies along the MFEP (sequence of red arrows in Figure 7C) show that the transition occurs through a single-step process, where the aggregates continuously transform into the swelled homogeneous brush. Interestingly, these results show that when the transformation between two morphologies is started from a state that is not a local minima of the free energy, the forward and reverse transitions (which occur on different free-energy hypersurfaces since ε is different in each case) can be qualitatively different.

View Article Online
DOI: 10.1039/C6SM02725C

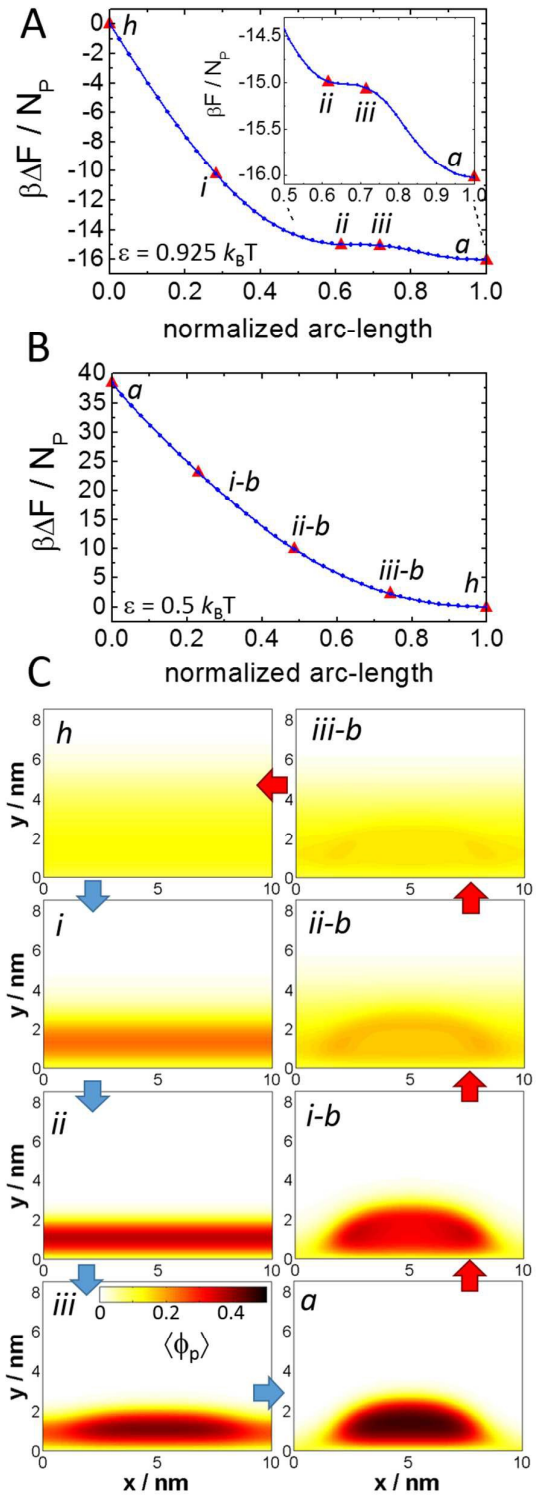

Figure 7: A. Minimum free-energy path for $\varepsilon = 0.925\ k_BT$ for the transition from a homogeneous brush (*h*) equilibrated at $\varepsilon = 0.5\ k_BT$ to self-assembled aggregates (*a*) equilibrated at $\varepsilon = 0.875\ k_BT$. B. Minimum free-energy path for $\varepsilon = 0.5\ k_BT$ from self-assembled aggregates (*a*) equilibrated at $\varepsilon = 0.925\ k_BT$ to a homogeneous brush (*h*) equilibrated at $\varepsilon = 0.5\ k_BT$. Note that in the MFEPs of panels A and B the initial state is not a local minima of the free energy. C. Color maps showing the volume fraction of the polymer for the morphologies indicated with red triangles in panels A and B. Blue and red arrows indicate the sequence of morphologies in the MFEPs of panels A and B, respectively. Calculation parameters $L = 50$, $N_P/A = 0.1$ chains·nm^{-2}.

Adhesion of Polymer Brushes on Opposing Surfaces

In addition to the $h \rightarrow a$ transition on a flat surface, we also used the molecular theory/string method introduced in this work to study the adhesion between two opposing surfaces modified by identical polymer brushes in a poor solvent, see scheme in Figure 8A. This configuration is typically found in adhesion experiments using AFM-colloidal probe[45-49] and Surface Force Apparatus experiments,[49] where the tethering surface can be approximated as planar in the length scale of the self-organized aggregates (~ 10 nm). Interestingly, experimental force-distance curves where one[46, 47] or both[45, 48, 49] surfaces are modified by hydrophobic polymers display hysteresis (the approaching and retracting curves are different).

In a previous work,[15] it has been shown that the molecular theory predicts, in fact, that the system depicted in Figure 8A can have two local free-energy minima for the same conditions: the self-organized aggregates (panel *a* in Figure 8C), where each surface is coated by assemblies like those described above for a single surface and the bridge morphology (panel *b* in Figure 8C), where the polymers bridge both surfaces. These two morphologies have been also predicted by scaling arguments[30] and computer simulations.[50] Figure 8B shows the MFEP curve for the $b \rightarrow a$ transition. In this particular case, the aggregates are more stable than the bridge by 0.06 k_BT/chain (1.2 k_BT/aggregate), but the transition requires to surpass a barrier of 0.17 k_BT/chain (3.4 k_BT/aggregate). This calculation suggests that the bridge morphology may exist as a metastable structure, which may contribute to the observed hysteresis in experimental force-distance curves. Figure 8C also shows the morphology of the system just before the barrier (panel *i*), at the barrier (panel *ii*) and just after the barrier (panel *iii*). These results show that the transition is predicted to occur by progressively thinning the bridge between both surfaces, until it breaks just at the position of the barrier (panel *ii*).

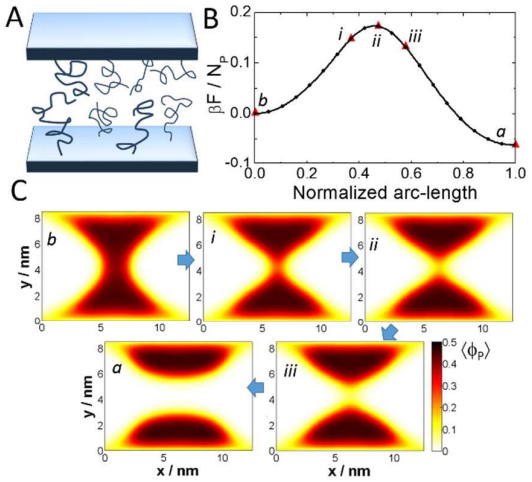

Figure 8: A. Scheme of a system comprising two planar opposing surfaces modified by identical end-grafted polymer layers. B. Minimum free-energy path from a morphology that bridges the two surfaces (*b*) to a morphology comprising

View Article Online
DOI: 10.1039/C6SM02725C

aggregates on both surfaces (*a*). These morphologies correspond to two different local minima of the free energy for the calculation conditions (L = 60, N_P/A = 0.1 chains·nm^{-2}, ε = 0.925 k_BT). C. Color maps showing the volume fraction of the polymer for the morphologies indicated with red triangles in B.

Conclusions

In this work, we have introduced a new implementation of the improved string method within the framework of a molecular theory. We used this theoretical tool to study the minimum free-energy paths (MFEPs) involved in the self-organization of polymer brushes. We studied first the microphase separation transition between the homogeneous brush and self-organized aggregates and showed that this transition may be barrierless or require to surpass a free-energy barrier. In the latter case, the transition is expected to procced via the nucleation of a cluster of a few aggregates within the homogeneous brush.[39] In the present work, we cannot observe this critical cluster as we performed studies at the level of a single aggregate; in the future, we plan to extend our calculations to larger systems in order to provide a more detailed characterization of the barrier state. We are also interested in performing calculations allowing inhomogeneities in three spatial directions,[1, 15] which would allow us to consider transitions between aggregates of different shape (micelles, stripes and solvent-filled holes).

We predict that both the homogeneous brush and the self-organized aggregates can exist as metastable structures. The experimentally observable consequence of this prediction will be the presence of hysteresis in the properties of the system when the quality of the solvent is changed. Actually, it is interesting to mention that experimentally measured properties of thermoresponsive polymers[51-53] and weak polyelectrolytes,[54] such as solvent uptake, density distribution and brush thickness, exhibit hysteresis when the quality of the solvent is varied by scanning temperature or pH. In other example, the properties of a weak polyelectrolyte brush immersed in a poor solvent were shown to differ depending on whether pre-treatment step in good solvent was used or not.[23] In Figure 5, we showed that the height of the barrier for the transition between aggregates and a homogeneous brush increases with increasing chain length, which suggests the existence of a minimum chain length below which the free-energy barrier will be too small to produce hysteresis within the experimental timescale. Interestingly, Varma et al.[53] studied the collapse/swelling transition of pNIPAM brushes as a function of the degree of polymerization and found hysteresis only when the chain length was longer than 260 segments/chains. Moreover, the magnitude of the hysteresis increased for increasing chain length. While the experiments discussed in this paragraph demonstrate the existence of hysteresis in the properties of polymer and polyelectrolyte brushes when the quality of the solvent is cycled, the morphology changes during such cycles were not characterized and therefore whether or not the observed hysteresis can be attributed to the formation of metastable morphologies remain an open question.

The molecular theory has some strengths that make it well-suited to be combined with the string method to study polymer brushes. Firstly, it incorporates molecular details of all the chemical species in the system, such as shape, flexibility and volume. The theory explicitly considers different molecular conformations and, therefore, unlike Gaussian chains, the chains have finite extension even in the presence of very strong stretching forces. This characteristic is important in the case of the system with two opposing polymer-modified surfaces studied here, where chains forming the bridge between surfaces are highly stretched. Secondly, the molecular theory allows for a straightforward estimation of the free energy of the system by evaluating the free-energy functional, in contrast to simulation methods that required computationally expensive thermodynamic integration calculations. Finally, we would like to mention that the molecular theory have been used in the past to investigate several soft-matter systems besides self-organizing polymer brushes, such as lipid bilayers,[55] hydrogels[56] and layer-by-layer films.[57] We expect that the molecular theory/string method introduced here will be applied in the future to these and other systems and thus become an integral part of the toolbox available to study self-organization in soft materials.

Acknowledgements

The authors acknowledge CONICET and Argentine National System for High Performance Computing (SNCAD-MinCyT) for access to the computer cluster at Centro de Cómputos de Alto Rendimiento-CONICET Rosario. MT gratefully acknowledges financial support from Agencia Nacional de Promoción Científica y Tecnológica (ANPCyT) (PICT-2015-0099), Prof. Igal Szleifer for his support and the use of his computer cluster in some of the calculations and Prof. Marcus Müller for an insightful discussion. EM acknowledges support from Stic-AmSud, CONICET-PIO (13320150100020CO), PICT-2015-2761, PICT-2015-0370, UTN3949 and UBACyT 20020130200096BA. MT and EM are fellows of CONICET.

Notes and references

1. M. Tagliazucchi, M. O. de la Cruz and I. Szleifer, *Proc. Natl. Acad. Sci. U.S.A.*, 2010, **107**, 5300-5305.
2. M. A. C. Stuart, W. T. Huck, J. Genzer, M. Müller, C. Ober, M. Stamm, G. B. Sukhorukov, I. Szleifer, V. V. Tsukruk and M. Urban, *Nat Mater*, 2010, **9**, 101-113.
3. F. Tantakitti, J. Boekhoven, X. Wang, R. V. Kazantsev, T. Yu, J. Li, E. Zhuang, R. Zandi, J. H. Ortony, C. J. Newcomb, L. C. Palmer, G. S. Shekhawat, M. O. de la Cruz, G. C. Schatz and S. I. Stupp, *Nat Mater*, 2016, **15**, 469-476.
4. J. M. Giussi, M. I. Velasco, G. S. Longo, R. H. Acosta and O. Azzaroni, *Soft Matter*, 2015, **11**, 8879-8886.
5. S. Ouk Kim, H. H. Solak, M. P. Stoykovich, N. J. Ferrier, J. J. de Pablo and P. F. Nealey, *Nature*, 2003, **424**, 411-414.
6. W. Li and M. Müller, *Annu. Rev. Chem. Biomol. Eng.*, 2015, **6**, 187-216.

View Article Online
DOI: 10.1039/C6SM02725C

7. F. S. Bates and G. H. Fredrickson, *Annu. Rev. Phys. Chem.*, 1990, **41**, 525-557.
8. A. Trent, R. Marullo, B. Lin, M. Black and M. Tirrell, *Soft Matter*, 2011, **7**, 9572-9582.
9. E. V. Shevchenko, D. V. Talapin, N. A. Kotov, S. O'Brien and C. B. Murray, *Nature*, 2006, **439**, 55-59.
10. M. E. Leunissen, C. G. Christova, A. P. Hynninen, C. P. Royall, A. I. Campbell, A. Imhof, M. Dijkstra, R. van Roij and A. van Blaaderen, *Nature*, 2005, **437**, 235-240.
11. O. Azzaroni, *J. Polym. Sci., Part A: Polym. Chem.*, 2012, **50**, 3225-3258.
12. S. K. Pattanayek, T. T. Pham and G. G. Pereira, *J. Chem. Phys.*, 2005, **122**, 214908.
13. S. K. Pattanayek and G. G. Pereira, *Macromol. Theory Simul.*, 2005, **14**, 347-357.
14. D. R. M. Williams, *J. Phys. II*, 1993, **3**, 1313-1318.
15. M. Tagliazucchi, X. Li, M. Olvera de la Cruz and I. Szleifer, *ACS Nano*, 2014, **8**, 9998-10008.
16. J.-M. Y. Carrillo and A. V. Dobrynin, *Langmuir*, 2009, **25**, 13158-13168.
17. D. J. Sandberg, J.-M. Y. Carrillo and A. V. Dobrynin, *Langmuir*, 2007, **23**, 12716-12728.
18. J. Wang and M. Müller, *J. Phys. Chem. B*, 2009, **113**, 11384-11402.
19. M. Müller, *Phys. Rev. E: Stat. Phys., Plasmas, Fluids,*, 2002, **65**, 030802.
20. V. Koutsos, E. W. vanderVegte, E. Pelletier, A. Stamouli and G. Hadziioannou, *Macromolecules*, 1997, **30**, 4719-4726.
21. B. C. Choi, S. Choi and D. E. Leckband, *Langmuir*, 2013, **29**, 5841-5850.
22. X. Gao, W. Feng, S. Zhu, H. Sheardown and J. L. Brash, *Langmuir*, 2008, **24**, 8303-8308.
23. M. Motornov, R. Sheparovych, E. Katz and S. Minko, *ACS Nano*, 2008, **2**, 41-52.
24. S. Minko, M. Müller, V. Luchnikov, M. Motomov, D. Usov, L. Ionov and M. Stamm, in *Polymer Brushes*, Wiley-VCH Verlag GmbH & Co. KGaA, 2005, DOI: 10.1002/3527603824.ch20, pp. 403-425.
25. D. Murakami, Y. Norizoe, Y. Higaki, A. Takahara and H. Jinnai, *Macromolecules*, 2016, **49**, 4862-4866.
26. R. M. Choueiri, E. Galati, H. Thérien-Aubin, A. Klinkova, E. M. Larin, A. Querejeta-Fernández, L. Han, H. L. Xin, O. Gang, E. B. Zhulina, M. Rubinstein and E. Kumacheva, *Nature*, 2016, **538**, 79-83.
27. T. F. Miller, E. Vanden-Eijnden and D. Chandler, *Proc. Natl. Acad. Sci. U.S.A.*, 2007, **104**, 14559-14564.
28. F. Lo Verso, L. Yelash, S. A. Egorov and K. Binder, *Soft Matter*, 2012, **8**, 4185-4196.
29. S. Santer, A. Kopyshev, J. Donges, H. K. Yang and J. Rühe, *Adv. Mater.*, 2006, **18**, 2359-2362.
30. E. B. Zhulina, T. M. Birshtein, V. A. Priamitsyn and L. I. Klushin, *Macromolecules*, 1995, **28**, 8612-8620.
31. O. Peleg, M. Tagliazucchi, M. Kroeger, Y. Rabin and I. Szleifer, *ACS Nano*, 2011, **5**, 4737-4747.
32. I. Szleifer and M. A. Carignano, *Adv. Chem. Phys.*, 1996, **96**, 165-260.
33. R. Nap, P. Gong and I. Szleifer, *J. Polym. Sci., Part B: Polym. Phys.*, 2006, **44**, 2638-2662.
34. W. E, W. Ren and E. Vanden-Eijnden, *J. Chem. Phys.*, 2007, **126**, 164103.
35. M. Müller, Y. G. Smirnova, G. Marelli, M. Fuhrmans and A.-C. Shi, *Phys. Rev. Lett.*, 2012, **108**, 228103.
36. C. L. Ting, D. Appelö and Z.-G. Wang, *Phys. Rev. Lett.*, 2011, **106**, 168101.
37. C. L. Ting and Z.-G. Wang, *Soft Matter*, 2012, **8**, 12066-12071.
38. W. Li and M. Müller, *Macromolecules*, 2016, **49**, 6126-6138.
39. X. Cheng, L. Lin, W. E, P. Zhang and A.-C. Shi, *Phys. Rev. Lett.*, 2010, **104**, 148301.
40. M. Müller and D.-W. Sun, *Phys. Rev. Lett.*, 2013, **111**, 267801.
41. S.-M. Hur, V. Thapar, A. Ramírez-Hernández, G. Khaira, T. Segal-Peretz, P. A. Rincon-Delgadillo, W. Li, M. Müller, P. F. Nealey and J. J. de Pablo, *Proc. Natl. Acad. Sci. U.S.A.*, 2015, **112**, 14144-14149.
42. W. E, W. Ren and E. Vanden-Eijnden, *Phys. Rev. B: Condens. Matter*, 2002, **66**, 052301.
43. L. Maragliano and E. Vanden-Eijnden, *Chem. Phys. Lett.*, 2007, **446**, 182-190.
44. M. Rubinstein and R. H. Colby, *Polymer Physics*, Oxford University Press, Oxford, 2003.
45. E. Svetushkina, N. Puretskiy, L. Ionov, M. Stamm and A. Synytska, *Soft Matter*, 2011, **7**, 5691-5696.
46. N. Ishida and M. Kobayashi, *J. Colloid Interface Sci.*, 2006, **297**, 513-519.
47. Y.-H. Lin, J. Teng, E. R. Zubarev, H. Shulha and V. V. Tsukruk, *Nano Lett.*, 2005, **5**, 491-495.
48. Y. Yu, B. D. Kieviet, E. Kutnyanszky, G. J. Vancso and S. de Beer, *ACS Macro Letters*, 2015, **4**, 75-79.
49. I. B. Malham and L. Bureau, *Langmuir*, 2010, **26**, 4762-4768.
50. S. de Beer, G. D. Kenmoé and M. H. Müser, *Friction*, 2015, **3**, 148-160.
51. S. Balamurugan, S. Mendez, S. S. Balamurugan, M. J. O'Brien and G. P. López, *Langmuir*, 2003, **19**, 2545-2549.
52. M. Annaka, C. Yahiro, K. Nagase, A. Kikuchi and T. Okano, *Polymer*, 2007, **48**, 5713-5720.
53. S. Varma, L. Bureau and D. Débarre, *Langmuir*, 2016, **32**, 3152-3163.
54. J. D. Willott, T. J. Murdoch, B. A. Humphreys, S. Edmondson, G. B. Webber and E. J. Wanless, *Langmuir*, 2014, **30**, 1827-1836.
55. M. J. Uline, G. S. Longo, M. Schick and I. Szleifer, *Biophys. J.*, 2010, **98**, 1883-1892.
56. G. S. Longo, M. Olvera De La Cruz and I. Szleifer, *ACS Nano*, 2013, **7**, 2693-2704.
57. G. Zaldivar and M. Tagliazucchi, *ACS Macro Letters*, 2016, **5**, 862-866.

View Article Online
DOI: 10.1039/C6SM02725C

Table of Contents

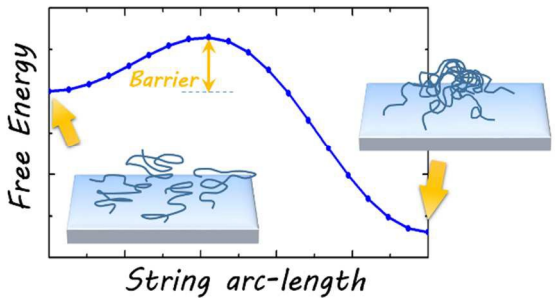

The mechanisms of self-organization of polymer brushes is poor solvent conditions have been studied with a newly developed molecular theory for minimum free-energy paths.